Nonlinear spectroscopy of Sr atoms in an optical cavity for laser stabilization

Bjarke T. R. Christensen,[1,*] Martin R. Henriksen,[1] Stefan A. Schäffer,[1] Philip G. Westergaard,[2] David Tieri,[3] Jun Ye,[3] Murray J. Holland,[3] and Jan W. Thomsen[1]

[1]*Niels Bohr Institute, University of Copenhagen, Blegdamsvej 17, 2100 Copenhagen, Denmark*
[2]*Danish Fundamental Metrology, Matematiktorvet 307, 1. sal, 2800 Kgs. Lyngby, Denmark*
[3]*JILA, National Institute of Standards and Technology and University of Colorado, Boulder, Colorado 80309-0440, USA*
(Received 21 July 2015; published 6 November 2015)

We study the nonlinear interaction of a cold sample of ^{88}Sr atoms coupled to a single mode of a low finesse optical cavity in the so-called bad cavity limit, and we investigate the implications for applications to laser stabilization. The atoms are probed on the weak intercombination line $|5s^2\,^1S_0\rangle - |5s5p\,^3P_1\rangle$ at 689 nm in a strongly saturated regime. Our measured observables include the atomic induced phase shift and absorption of the light field transmitted through the cavity represented by the complex cavity transmission coefficient. We demonstrate high signal-to-noise-ratio measurements of both quadratures—the cavity transmitted phase and absorption—by employing frequency modulation (FM) spectroscopy (noise-immune cavity-enhanced optical-heterodyne molecular spectroscopy). We also show that when FM spectroscopy is employed in connection with a cavity locked to the probe light, observables are substantially modified compared to the free-space situation in which no cavity is present. Furthermore, the nonlinear dynamics of the phase dispersion slope is experimentally investigated, and the optimal conditions for laser stabilization are established. Our experimental results are compared to state-of-the-art cavity QED theoretical calculations.

I. INTRODUCTION

Lasers with exceedingly pure spectral features are a key element in the interrogation of ultranarrow atomic transitions applied in, for example, optical atomic clocks [1–5], condensed-matter simulations with cold atoms [6], and relativistic geodesy [7,8]. Such pure spectral instruments with high-phase stability and long coherence times are essential to investigations of physics beyond the standard model, e.g., the drift of fundamental physical constants [9,10] or the detection of gravitational waves [11] as predicted by the general theory of relativity. The stability of the current state-of-the-art lasers is limited by Brownian motions of the reference cavity mirror substrates and coatings [12–14], and the emergence of new technologies [15–17] seems necessary if further improvements are to be made commonly available.

Recent studies have proposed a new scheme for laser stabilization to a mK thermal sample of atoms placed in a low finesse optical cavity [18–21]. By placing the atoms inside the optical cavity, atom-light interactions are enhanced by order of the finesse of the cavity, and nonlinear effects are brought into play, which enhance the spectral sensitivity of the detected photocurrent used for stabilization. Interestingly, the first proposals considered atoms trapped in an optical lattice or systems with a sample temperature equivalent to zero degrees Kelvin [19]. Further studies have extended these results to also include the finite temperature of the sample [20,21]. At finite temperatures, the bistability regime, present at the optimal locking point for zero-Kelvin systems, turns out to be effectively removed. Since there is no bistability at the optimal locking point for finite-temperature systems, this sparks renewed interest for stabilization to samples of atoms with finite temperatures.

In this work, we investigate the nonlinear coupling of laser-cooled ^{88}Sr atoms to a single mode of an optical cavity. During experiments, the atom-modified cavity mode is forced to be on-resonance with the carrier of the probe laser and thus a standing wave will be present at all times in the cavity. As a result, significant changes appear in the observables of the system due to reaction of the atoms on the cavity servo system.

This has major consequences: the phase and absorption information is altered compared to conventional free-space frequency modulation (FM) spectroscopy, but may be recovered under special conditions of laser detuning and demodulation frequency. In the following, we also explore the nonlinear cavity-atom dynamics and identify optimal parameters relevant for laser stabilization to our cavity system. The experiments are performed in a cyclic manner, but the understanding of the nonlinear dynamics and the optimal experimental parameters obtained here will prove valuable for continuous laser stabilization to future noncyclic systems [22].

II. EXPERIMENTAL SETUP

Experimentally, our cavity system consists of a sample of laser-cooled ^{88}Sr atoms with a temperature of 5 mK coupled to an optical cavity with finesse $F = 85$; see Fig. 1(a). We operate a standard magneto-optical trap (MOT) and trap about 5×10^8 Sr atoms using the strong $^1S_0 \rightarrow {}^1P_1$ transition at 461 nm; see Fig. 1(b). The system is probed on the $^1S_0 \rightarrow {}^3P_1$ intercombination transition at 689 nm while the cavity is forced to be on resonance with the probe laser at all times. The cavity mirrors have a radius of curvature of 9 m yielding a cavity waist diameter of about 1 mm, which is comparable to the size of the MOT. At our current MOT temperature, we estimate the transit time broadening to be 1–2 kHz, which is significantly smaller than the natural atomic linewidth of $\Gamma/2\pi = 7.5$ kHz. The 30 cm cavity, with a free spectral range (FSR) of 500 MHz, is placed outside the vacuum chamber

*bjarkesan@nbi.ku.dk
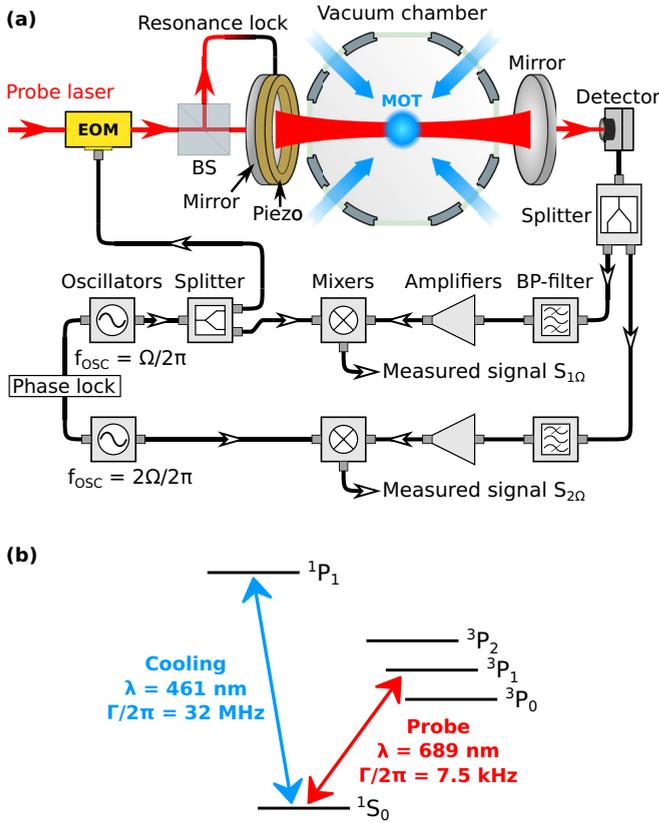
FIG. 1. (Color online) (a) Experimental setup. A sample of cold ^{88}Sr atoms trapped in a standard magneto-optical trap (MOT) is located inside a low finesse optical cavity ($F = 85$). The cavity is locked to resonance with the light using the Hänsch-Couillaud [25] scheme. We perform cavity-enhanced FM spectroscopy (NICE-OHMS) where the light is modulated at $\Omega/2\pi =$ FSR (free spectral range of the cavity). The detected signal is split into two arms where the Ω and 2Ω components are selected by band-pass filters and separately demodulated using rf mixers. One part of the signal is demodulated at Ω giving a phase signal, and the other part is demodulated at 2Ω giving an attenuation signal. Both the phase shift and the absorption line shape of the transmitted probe light are recorded simultaneously with this scheme. (b) Energy levels of the ^{88}Sr atom important for this work. The singlet transition $|5s^2\,^1S_0\rangle - |5s5p\,^1P_1\rangle$ at 461 nm is used to trap and cool the atoms. The narrow intercombination line transition $|5s^2\,^1S_0\rangle - |5s5p\,^3P_1\rangle$ at 689 nm is used to probe the atoms.

thereby limiting the obtainable finesse. We measure a cavity linewidth of $\kappa/2\pi = 5.8$ MHz placing our system in the bad-cavity regime $\kappa \gg \Gamma$. We probe the atoms for 100 μs and the 461 nm light is turned off during this probing period. At the probing time scale, our prestabilized laser has an estimated linewidth of 800 Hz.

We employ cavity-enhanced FM spectroscopy [noise-immune cavity-enhanced optical-heterodyne molecular spectroscopy (NICE-OHMS)] [23,24]; see Fig. 1, where the probe carrier is modulated at the FSR to create sidebands, in our case separated from the carrier by multiples of 500 MHz. The cavity-transmitted signal is detected by a high bandwidth photodetector recording the beat note between the carrier

and the sidebands. This signal contains information about the cavity-transmitted field amplitude and nonlinear phase shifts due to the atoms present in the cavity. These contributions are recovered with a high signal-to-noise ratio by demodulating at FSR and multiple FSRs.

Our cavity system supports a single-atom cooperativity $C_0 = 4g^2/\Gamma\kappa$ of $C_0 = 3 \times 10^{-5}$, where g is the single-atom-cavity coupling constant. For our cavity setup, we find $g/2\pi = 590$ Hz. The C_0 parameter is a measure of the rate at which an atom emits a photon into the cavity mode compared to all other dissipation rates in the system. For the collective cooperativity, we find $C = N_{\mathrm{cav}}C_0 = 630$, where N_{cav} is the total number of atoms in the cavity mode volume. With a MOT atom number of 5×10^8, we find $N_{\mathrm{cav}} = 2.5 \times 10^7$.

III. THEORY OF MEASUREMENT

In this section, we establish a connection between our measured cavity-transmitted quantities and the complex transmission coefficient of the input field χ. Our input probe field can be written in terms of a carrier and multiple orders of sidebands induced by phase modulation. By neglecting residual amplitude modulation, the total input probe field, E_{in}, with sidebands can be given as

$$E_{\mathrm{in}} = E_0 \sum_{p=-\infty}^{\infty} J_p(x)e^{i(\omega_c + p\Omega t)}, \tag{1}$$

where $J_p(x)$ is the pth-order regular Bessel function describing the amount of power transferred from the carrier ($p = 0$) to the sidebands ($|p| > 0$), x is the electro-optic modulator (EOM) modulation index, ω_c is the carrier frequency, which is close to the atomic resonance, and Ω is the EOM modulation frequency equal to the free spectral range of the cavity. Each transmitted component of the cavity field is modified by the cavity according to the well-known expression [26]

$$E_{\mathrm{out}} = \frac{Te^{i\varphi}}{1 - Re^{i2\varphi}}E_{\mathrm{in}} = \chi E_{\mathrm{in}}, \tag{2}$$

where χ is the complex transmission coefficient describing the phase change and the absorption of the field, T (R) is the power transmission (reflection) coefficient of the cavity mirrors, and φ is the single round-trip complex phase picked up by the intracavity field.

The carrier frequency is used to probe the atomic transition and is close to the atomic resonance, while the sidebands at $\Omega/2\pi = 500$ MHz are far off resonance compared to the natural linewidth, $\Gamma/2\pi = 7.5$ kHz. Each of the field's phase components—carrier (φ_0) and sidebands ($\varphi_{\pm p}$ for $p = 1,2$)—experiences identical phase shifts due to the cavity assembly ϕ_{cavity}, but only the carrier interacts with the atoms,

$$\varphi_0 = \phi_{\mathrm{cavity}} + \beta_D + i\beta_A, \quad \varphi_{\pm p} = \phi_{\mathrm{cavity}} \pm p\pi, \tag{3}$$

where β_D and β_A denote the single pass dispersion and absorption due to the atoms present in the cavity, and the sideband frequency detuning of $\pm p\Omega$ introduces additional phase factors of $\pm p\pi$ if the cavity is on resonance with the carrier and the sidebands. During experiments, the cavity is forced to be on resonance with the probe laser, a requirement that generally imposes restrictions on measured quantities

in cavity experiments. Enforcing the resonance condition by locking the cavity to the probe carrier implies

$$\text{Re}(\varphi_0) = \theta_0 = \phi_{\text{cavity}} + \beta_D = m\pi, \qquad (4)$$

where θ_0 is the real part of φ_0 and m is an integer. This imposes restrictions on the sideband phases, which become

$$\varphi_{\pm p} = \phi_{\text{cavity}} - \theta_0 \pm p\pi = -\beta_D \pm p\pi. \qquad (5)$$

For the carrier, the complex transmission coefficient χ_0 becomes purely real,

$$\chi_0 = \frac{T e^{-\beta_A}}{1 - R e^{-2\beta_A}}, \qquad (6)$$

while the sideband complex transmission coefficients $\chi_{\pm p}$ become

$$\chi_{\pm p} = \frac{T e^{i(\pm p\pi - \beta_D)}}{1 - R e^{2i(\pm p\pi - \beta_D)}}, \qquad (7)$$

and the atomic phase shift β_D is transferred onto the sideband transmission coefficients. As the cavity is kept on resonance with the carrier at all times, we obtain the final output field to second order, E_{out}:

$$
\begin{aligned}
E_{\text{out}} = E_0 (& J_0(x)\chi_0 e^{i\omega_c t} \\
& + J_1(x)\chi_1 e^{i(\omega_c + \Omega)t} - J_1(x)\chi_{-1} e^{i(\omega_c - \Omega)t} \\
& + J_2(x)\chi_2 e^{i(\omega_c + 2\Omega)t} + J_2(x)\chi_{-2} e^{i(\omega_c - 2\Omega)t}). \quad (8)
\end{aligned}
$$

Detecting this signal on a fast photodiode and demodulating at $\Omega/2\pi = \text{FSR}$ gives a photocurrent signal $S_{1\Omega}$ proportional to

$$S_{1\Omega} \propto J_0(x)J_1(x)\chi_0 \text{Im}(\chi_1), \qquad (9)$$

where $\text{Im}(\chi_1)$ is the imaginary part of the χ_1 coefficient.

In the limit $R \to 0$, corresponding to the free space case in which no cavity is used, we recover from Eq. (9) the well-known expression from FM spectroscopy $S_{1\Omega} \propto e^{-\beta_A} \sin(\beta_D)$. On the other hand, in the limit where the complex phase shift due to the atoms is very small, i.e., $\beta_D \to 0$ and a cavity is present, we find $S_{1\Omega} \propto \beta_D$, which is also proportional to the total atomic phase shift of the transmitted sideband field. In our case, this approximation is satisfied very close to resonance.

Information related to the absorption of the transmitted light may be obtained by demodulating the transmitted field at twice the FSR, i.e., 2Ω, where one obtains (here with sidebands up to second order)

$$S_{2\Omega} \propto \left[2J_0(x)J_2(x)\chi_0 \text{Re}(\chi_2) - J_1^2(x)|\chi_1|^2 \right], \qquad (10)$$

where $\text{Re}(\chi_2)$ is the real part of the χ_2 coefficient. This signal is related to the absorption line shape of the transmitted field (see Appendix). The complete information about the complex transmission coefficients, χ_j, can now be found by combining the quantities obtained from demodulating at FSR and 2FSR via Eqs. (9) and (10).

In conclusion, the demodulating of the cavity-transmitted field by $\Omega/2\pi = \text{FSR}$ [Eq. (9)] provides a signal proportional to the atomically induced phase shift for small detunings. The high signal-to-noise-ratio of this signal makes it promising for applications in laser stabilization. The absorption line shape, on the other hand, can be obtained by demodulating the cavity-transmitted field by 2FSR [Eq. (10)]. This technique can

also be applied to molecular systems at ambient temperatures coupled to optical cavities, and it is not only limited to laser-cooled neutral atoms.

IV. RESULTS AND DISCUSSION

In our system, the energy scale associated with the mK Doppler temperature is several orders of magnitude larger than the energy scale associated with the narrow linewidth of the optical transition. In this limit, the nonzero velocities of the atoms bring additional multiphoton resonance phenomena into play, so-called doppleron resonances, which modify the complex transmission coefficient of the cavity field close to the atomic resonance [21].

Doppleron resonances are multiphoton processes in which $l + 1$ photons from one direction are resonantly absorbed by an atom with a velocity v, and l photons are emitted in the reverse direction leaving the atom in the excited state [27,28]. Energy conservation demands the doppleron resonances to be located approximately at [27]

$$kv = \frac{\pm(\Delta^2 + 2g^2)^{1/2}}{2l + 1}, \qquad (11)$$

where k is the wave vector of the laser light, v is the resonant atom velocity, Δ is the detuning, l is the number of emitted photons, i.e., the order of the doppleron resonance, and g is the single-atom-cavity coupling constant.

NICE-OHMS signals obtained by demodulation at $\Omega/2\pi = \text{FSR}$, see Eq. (9), are shown in Fig. 2(a). Those values represent the total phase dispersion induced by the atom-cavity system. A sharp dispersion signal with a steep slope can be seen around resonance. The magnitude of this slope, as well as the signal-to-noise ratio, ultimately determines the obtainable frequency stability of the system when used as a frequency discriminator for laser stabilization. The inset in Fig. 2(a) shows a zoom of the central dispersion curve close to resonance. This NICE-OHMS signal is proportional to the cavity-transmitted phase shift. Two theoretical plots are also shown. The blue solid line displays the full theory, i.e., including doppleron resonances to all orders, while the black dashed line is based on a theoretical prediction where the velocity-dependent doppleron resonances are not taken into account. We observe very good agreement with the full theoretical model including all doppleron orders, and we notice that the doppleron resonances tend to decrease the phase dispersion slope around resonance slightly. The two theory lines are also included in the broad frequency scan shown in Fig. 2(a). For the dashed theory line excluding doppleron resonances, the agreement with the data is always worse than that including the doppleron resonances.

Whereas the results presented in Fig. 2(a) have already been understood in previous works [21], the corresponding absorption line shape has not yet been fully understood. The signal obtained by demodulating the cavity-transmitted field at 2FSR [Eq. (10)] is shown in Fig. 2(b) and is related to the absorption line shape of the cavity-transmitted field. A background signal corresponding to the empty cavity signal (no atoms) is subtracted. A similar background value has been subtracted from the theoretical values. The absolute value of this background-corrected signal represents the degree of
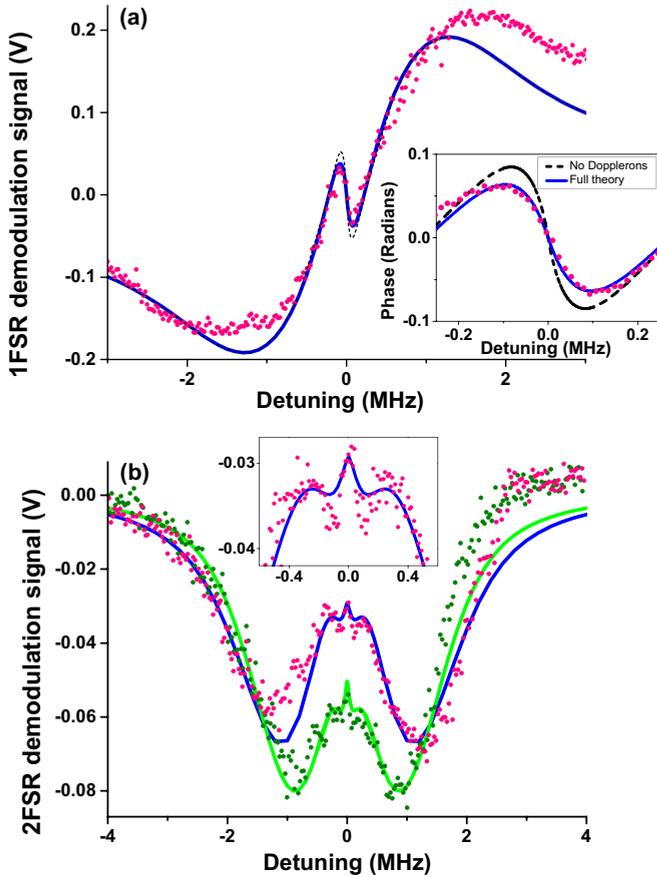
FIG. 2. (Color online) The solid and dashed lines are predictions based on the theoretical model presented in [20,21]. The dots are data measured by cavity-enhanced FM spectroscopy. All data are averaged values, where approximately five times as many measurements have been performed for data in (b) due to the weaker signal compared to data in (a). The slight asymmetry of the experimental data in both plots is expected to be due to a drift of the relative phase between the light wavefront and the demodulation phase during scan. (a) Frequency scan of the cavity-transmitted phase shift close to resonance for a carrier input power of 240 nW, a total number of atoms of $N = 5.0 \times 10^8$, and an atom temperature of $T = 5.0$ mK. The data points are averages of nine measurements. Theoretical values from Eq. (9) are scaled to data. Inset: high-resolution scan of the central region. The vertical axis in this central region corresponds to the total atomic phase shift of the transmitted sideband, and data are scaled to theory. (b) Frequency scans of the absorption line shape of the cavity-transmitted field measured by the NICE-OHMS technique obtained with a demodulation $\Omega/2\pi = 2$FSR. The total number of atoms is $N = 4.5 \times 10^8$, an atom temperature of $T = 5.0$ mK, and a total input power of 310 nW (blue line) and 155 nW (green line). Theoretical values from Eq. (10) are scaled to data. Inset: high-resolution scans around the central region. The units on the inset axes are the same as in (b).

field absorption experienced by light transmitted through the cavity. To reproduce the detailed features of the absorption line shape, we must include contributions from sidebands up to the third order in the theoretical model. These higher-order contributions modify the line shape. Different modulation indices of $x = 0.65$ for the blue theory line and of $x = 0.57$

for the green theory line are chosen to show that the signal described in Eq. (10) takes the optical power ratio of the carrier and the sidebands into account, in good agreement with the data.

The absorption line shapes in Fig. 2(b) are shown for two different carrier input powers: 310 nW (red dots) and 155 nW (green dots). The 2FSR demodulation signal is proportional to the total optical input power. A carrier input power of 155 nW should thus yield about half of the signal measured for a carrier input power of 310 nW. This is indeed observed experimentally, however in the presented figure the signal for a carrier input power of 155 nW has been normalized to the signal for a carrier input power of 310 nW in order to illustrate the line-shape dynamics on the same figure.

As mentioned earlier, the cavity is forced on resonance with the probe carrier by the cavity lock feedback loop such that the combined atom-cavity system is kept on resonance. However, the presence of several sideband orders contributes to the servo error signal for large atomic phase shifts and will slightly offset the cavity resonance compared to the carrier frequency [29]. Corrections due to these shifts are small, but they are included in the theoretical model for completeness.

The central region of Fig. 2(b) shows a small central peak with reduced absorption (increased transmission) due to saturation. Insets show a zoom of the phase and the cavity-transmitted signal in Figs. 2(a) and 2(b), respectively. A reduction in transmission occurs for small detunings and forms dips on both sides of the central saturation peak at around 100 kHz. This reduction is due to atom-induced cavity response, where a nonzero atomic phase shifts the sidebands out of cavity resonance and reduces the transmitted power. As the detuning increases to larger values, the phase shift induced by the atoms eventually decreases to zero again, bringing the sidebands back into resonance with the cavity mode and thus increasing the amount of transmitted light. This corresponds to the two shoulders located next to the dips. This structure is less pronounced when measuring the total cavity transmitted power as a function of the detuning because the carrier, which is kept on resonance, accounts for most of the transmitted power for low modulation indices ($x < 1$). On the other hand, this structure is significantly more pronounced when the cavity-transmitted field is demodulated with 2FSR [Eq. (10)]. A detailed account of this structure can be found in Appendix. The atom-induced cavity response seems even more pronounced in the data [see the inset in Fig. 2(b)] than predicted by theory, which might be due to an imperfect cavity-locking scheme.

The shot-noise limited linewidth of the system, $\Delta\nu$, can be estimated by assuming a perfect locking scheme that is of infinite bandwidth, and detectors with unity quantum efficiencies as [19]

$$\Delta\nu = \frac{\pi\hbar\nu}{2P_{\text{sig}}\left(\frac{d\phi}{d\nu}\right)^2}\left(1 + \frac{P_{\text{sig}}}{2P_{\text{sideband}}}\right), \qquad (12)$$

where P_{sig} is the input carrier power, P_{sideband} is the first-order sideband power, and $\frac{d\phi}{d\nu}$ is the dispersion slope at resonance. The minimum achievable shot-noise limited linewidth of the current system is estimated from Eq. (12) to be 500 mHz. The minimum shot-noise limited linewidth will be further reduced

for higher values of $C = NC_0$. Hence, it can be optimized by increasing the atom number or the cavity finesse.

A system with improved finesse ($F = 1000$) and intracavity atom number (N_{cav}) increased by a factor 2 is estimated to have a shot-noise limited linewidth of $\Delta \nu < 10$ mHz [20], which is already comparable to state-of-the-art laser stabilization [13,30,31], and even narrower linewidths can be expected for a higher cavity finesse realized for intravacuum cavities in similar works [15]. Furthermore, the theoretical model shows that the gain, in terms of dispersion slope $\frac{d\phi}{d\nu}$, by further cooling of the atomic sample is minimal [21]. Experimentally, the reduction of the sample temperature by one or two orders of magnitude in temperature is usually accompanied by a reduction in atom number by similar orders of magnitude. In this regime with lower temperature, the optimum input power is reduced to technically challenging values (<nW). Therefore, the overall gain from reducing the sample temperature and thereby increasing the complexity of the system is comparatively small, and operating the system at relatively high temperature is more desirable. This may pave the way for implementations of thermal atoms in a simple and compact transportable optical atomic clock with high phase stability.

The phase dispersion slope depends nonlinearly on the optical intracavity power, which makes the optimal choice of parameters for laser stabilization nontrivial. The nonlinear input power dependence of the phase dispersion slope is measured and shown in Fig. 3(a). The slope values are evaluated by performing theoretical fits on phase dispersion scans, shown in Figs. 3(c)–3(e), for different input powers. The measurements and theory are in good agreement, and the nonlinear input power dependency predicted in [20] is evident. The theoretical curve predicts a maximum absolute value of the slope for lower input powers than measured. However, the shot-noise limited linewidth does not depend solely on the phase dispersion slope. It is also governed by the input power in accordance with Eq. (12). The shot-noise limited linewidth for each measured parameter is calculated and shown in Fig. 3(b), where data sets in Figs. 3(a) and 3(b) are identical. Figure 3(b) shows that a system with input powers corresponding to the predicted minimum shot-noise limited linewidth has been realized and measured for a fixed carrier-sideband ratio. Note that the horizontal axis is logarithmic, allowing a change in input power of one order of magnitude without degrading the shot-noise limited linewidth significantly. This indicates that probing with technically challenging low input powers down to <100 nW is not necessary, and that the system is robust to changes in the input power. The ratio of carrier and sideband powers is governed by the modulation index x of the EOM, and it optimizes the linewidth in Eq. (12) for a carrier-sideband ratio of $\frac{P_{sig}}{2P_{sideband}} = 1$. The measurements presented in this work are performed in a cyclic manner, and continuous laser stabilization on the presented system is not currently feasible. However, the implementation of the techniques presented in this work into beamline experiments [22], where a beam of cold atoms with high loading rates [32] is interrogated in a cavity, seems realizable. This paves the way for a continuous laser stabilization on an atom-cavity system with a narrow optical transition.
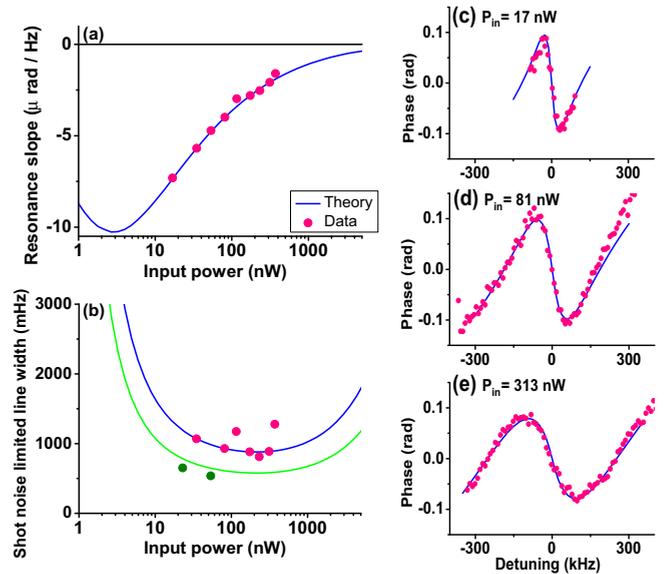
FIG. 3. (Color online) The input power dependence of the slope of the phase dispersion around resonance and the corresponding shot-noise limited linewidth for a total number of atoms of $N = 4.0 \times 10^8$ and MOT temperature of $T = 5.0$ mK. The solid lines are theoretical predictions and the dots are experimental data. (a) The slope of the phase dispersion around resonance measured for different input powers. The data and theory are in excellent accordance and the nonlinear dependence is evident. Notice that the power axis is logarithmic. (b) The shot-noise limited linewidth from Eq. (12) for different input powers corresponding to the measured parameters in (a). The solid lines are theoretical predictions and the dots are experimental values. The blue theory line corresponds to a ratio of carrier and sideband input powers of $\frac{P_{sig}}{2P_{sideband}} = 1.65$ and the green theory line corresponds to $\frac{P_{sig}}{2P_{sideband}} = 0.75$. (c)–(e) Frequency scans of the phase dispersion for different input powers. All experimental values in (a) and (b) are evaluated by fitting theoretical curves to frequency scans of the phase dispersion around resonance. The nonlinear dynamics of the overall dispersion shape is in very good accordance with the theory.

V. CONCLUSION

We have experimentally investigated the velocity-dependent spectroscopic features and nonlinear dynamics of a cavity-atom system in the bad-cavity limit consisting of laser-cooled ^{88}Sr atoms coupled to a low finesse optical cavity.

The NICE-OHMS technique has been applied to perform FM spectroscopy, and a complete connection is established between the measured quantities and the complex transmission coefficient of the input field. The cavity-transmitted phase shift and the absorption of the cavity-transmitted field are measured, and both quantities show significant modifications due to velocity-dependent processes and atom-induced cavity response in accordance with the theoretical model.

The ideal shot-noise limited linewidth of a laser stabilized to our system depends on the phase dispersion slope around resonance. The nonlinear input power dependence of the phase

dispersion slope is measured, and the optimal input power for the minimum shot-noise limited linewidth is determined. Parameters corresponding to a shot-noise limited linewidth down to 500 mHz are measured.

The understanding of relevant velocity-dependent effects presented here has direct relevance for atomic clocks and superradiant laser sources [18] involving ultranarrow transitions. Specifically, the understanding of the dynamics of a cavity-atom system with single-stage MOT temperatures obtained in this work will prove valuable for future transportable stable lasers and atomic clocks employing thermal atoms for out-of-lab operation under more noisy environments.

APPENDIX: LINE SHAPE OF ABSORPTION

The absorption dips shown in the inset of Fig. 2(b) are predicted from our theoretical model [20,21], where the empty cavity frequency is kept on resonance with the probe field. The standing-wave condition inside the cavity is, however, unfulfilled when a strong atomic dispersion is introduced, and the transmission will be reduced for all detunings with nonzero atomic phase shifts. Hence the large enhancement of the absorption for large detunings (∼MHz) is also due to the broad thermal dispersion.

Experimentally, the cavity servo system ensures that the combined resonance of the cavity and the atoms is kept on resonance with the probe field. The standing-wave condition is hence maintained and the atomic phase shift is canceled out for the carrier, as shown in Eq. (4). A measurement of the transmission power of the system will be dominated by the complex transmission coefficient of the carrier, χ_0 [see Eq. (6)], and the change in the transmission power due to
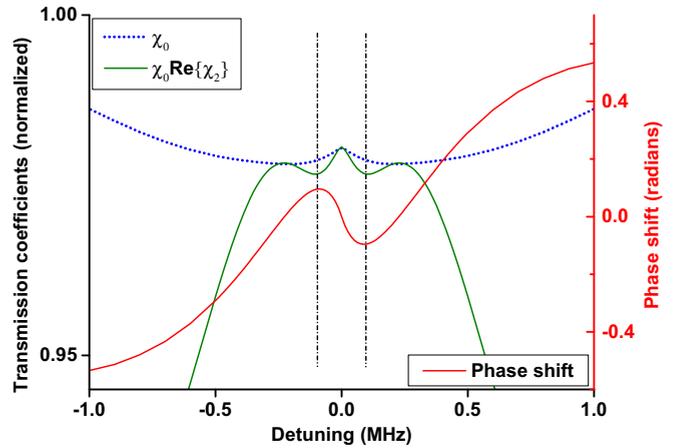
FIG. 4. (Color online) Theoretical values of the transmission coefficient of the carrier (dashed blue), χ_0, the combined line shape of the atomic absorption and the attenuation due to atomic dispersion (green), $\chi_0 \text{Re}\{\chi_2\}$, and the total cavity transmitted phase shift (red). The black vertical dashed lines highlight the fact that transmission minima occur at dispersion maxima.

the atomic phase shift is not evident. The signal demodulated with 2FSR [Eq. (10)], on the other hand, contains information about the atomic absorption (χ_0) and the attenuation due to the atomic phase shift [Re(χ_2)]. Hence, the detailed absorption structure is evident in this signal.

Theoretical values of some relevant transmission coefficients are shown in Fig. 4. χ_0 (blue line) describes only the atomic absorption of the carrier [see Eq. (6)], and $\chi_0\text{Re}(\chi_2)$ describes the combined line shape from the atomic absorption (χ_0) and the attenuation due to the atomic phase shift [Re(χ_2)]. $\chi_0\text{Re}(\chi_2)$ corresponds to the first term of Eq. (10) measured using the NICE-OHMS technique with demodulation of 2FSR. The second term in Eq. (10) and the additional contributions from the higher-order sidebands included in the theoretical description modify the line shape without erasing the structures. The corresponding total dispersion of the system is also shown in Fig. 4, and it is evident that the transmission minima occur at the dispersion maxima (highlighted with dashed vertical lines).

[1] B. J. Bloom *et al.*, An optical lattice clock with accuracy and stability at the 10^{-18} level, Nature (London) **506**, 71 (2014).

[2] T. L. Nicholson *et al.*, Systematic evaluation of an atomic clock at 2×10^{-18} total uncertainty, Nat. Commun. **6**, 6896 (2015).

[3] I. Ushijima *et al.*, Cryogenic optical lattice clocks, Nat. Phot. **9**, 185 (2015).

[4] N. Hinkley *et al.*, An atomic clock with 10^{-18} instability, Science **341**, 1215 (2013).

[5] R. Le Targat *et al.*, Experimental realization of an optical second with strontium lattice clocks, Nat. Commun. **4**, 2109 (2013).

[6] M. J. Martin *et al.*, A quantum many-body spin system in an optical lattice clock, Science **341**, 632 (2013).

[7] R. Bondarescu *et al.*, Geophysical applicability of atomic clocks: direct continental geoid mapping, Geophys. J. Int. **191**, 78 (2012).

[8] J. Guéna, M. Abgrall, D. Rovera, P. Rosenbusch, M. E. Tobar, P. Laurent, A. Clairon, and S. Bize, Improved Tests of Local Position Invariance Using ^{87}Rb and ^{133}Cs Fountains, Phys. Rev. Lett. **109**, 080801 (2012).

[9] T. Rosenband *et al.*, Frequency ratio of Al$^+$ and Hg$^+$ single-ion optical clocks; Metrology at the 17th decimal place, Science **319**, 1808 (2008).

[10] R. M. Godun, P. B. R. Nisbet-Jones, J. M. Jones, S. A. King, L. A. M. Johnson, H. S. Margolis, K. Szymaniec, S. N. Lea, K. Bongs, and P. Gill, Frequency Ratio of Two Optical Clock Transitions in ^{171}Yb$^+$ and Constraints on the Time Variation

of Fundamental Constants, Phys. Rev. Lett. **113**, 210801 (2014).

[11] P. W. Graham, J. M. Hogan, M. A. Kasevich, and S. Rajendran, New Method for Gravitational Wave Detection with Atomic Sensors, Phys. Rev. Lett. **110**, 171102 (2013).

[12] T. Kessler, T. Legero, and U. Sterr, Thermal noise in optical cavities revisited, J. Opt. Soc. Am. B **29**, 178 (2012).

[13] T. Kessler *et al.*, A sub-40-mHz-linewidth laser based on a silicon single-crystal optical cavity, Nat. Photon. **6**, 687 (2012).

[14] G. D. Cole *et al.*, Tenfold reduction of Brownian noise in high-reflectivity optical coatings, Nat. Photon. **7**, 644 (2013).

[15] M. A. Norcia and J. K. Thompson, Strong Coupling on a Forbidden Transition in Strontium and Nondestructive Atom Counting, arXiv:1506.02297.

[16] J. G. Bohnet *et al.*, A steady-state superradiant laser with less than one intracavity photon, Nature (London) **484**, 78 (2012).

[17] R. Kohlhaas, A. Bertoldi, E. Cantin, A. Aaspect, A. Landragin, and P. Bouyer, Phase Locking a Clock Oscillator to a Coherent Atomic Ensemble, Phys. Rev. X **5**, 021011 (2015).

[18] D. Meiser, J. Ye, D. R. Carlson, and M. J. Holland, Prospects for a Millihertz-Linewidth Laser, Phys. Rev. Lett. **102**, 163601 (2009).

[19] M. J. Martin, D. Meiser, J. W. Thomsen, J. Ye, and M. J. Holland, Extreme nonlinear response of ultranarrow optical transitions in cavity QED for laser stabilization, Phys. Rev. A **84**, 063813 (2011).

[20] D. A. Tieri, J. Cooper, B. T. R. Christensen, J. W. Thomsen, and M. J. Holland, Laser stabilization using saturated absorption in a cavity-QED system, Phys. Rev. A **92**, 013817 (2015).

[21] P. G. Westergaard, B. T. R. Christensen, D. Tieri, R. Matin, J. Cooper, M. Holland, J. Ye, and J. W. Thomsen, Observation of Motion-Dependent Nonlinear Dispersion with Narrow-Linewidth Atoms in an Optical Cavity, Phys. Rev. Lett. **114**, 093002 (2015).

[22] J. Chen, Active optical clock, Chin. Sci. Bull. **54**, 348 (2009).

[23] J. Ye, L.-S. Ma, and J. L. Hall, Ultrasensitive detections in atomic and molecular physics: demonstration in molecular overtone spectroscopy, J. Opt. Soc. Am. B **15**, 6 (1998).

[24] L.-S. Ma, J. Ye, P. Dubé, and J. L. Hall, Ultrasensitive frequency-modulation spectroscopy enhanced by a high-finesse optical cavity: theory and application to overtone transitions of C_2H_2 and C_2HD, J. Opt. Soc. Am. B **16**, 2255 (1999).

[25] T. W. Hänsch and B. Couillaud, Laser frequency stabilization by polarization spectroscopy of a reflecting reference cavity, Opt. Commun. **35**, 441 (1980).

[26] F. Riehle, *Frequency Standards: Basics and Applications* (Wiley-VCH, Weinheim, 2004).

[27] A. Tallet, Raman emission versus dopplerons in a two-level atomic cell, Soc. Am. B **11**, 1336 (1994).

[28] E. Kyrölä and S. Stenholm, Velocity tuned resonances as multi-doppleron processes, Opt. Commun. **22**, 123 (1977).

[29] J. Ye and T. W. Lynn, Applications of optical cavities in modern atomic, molecular, and optical physics, Adv. At., Mol., Opt. Phys. **49**, 1 (2003).

[30] M. Bishof, X. Zhang, M. J. Martin, and J. Ye, Optical Spectrum Analyzer with Quantum-Limited Noise Floor, Phys. Rev. Lett. **111**, 093604 (2013).

[31] S. Häfner *et al.*, 8×10^{-17} fractional laser frequency instability with a long room-temperature cavity, Opt. Lett. **40**, 2112 (2015).

[32] T. Yang *et al.*, A high flux source of cold strontium atoms, Eur. Phys. J. D **69**, 226 (2015).